Design and Construction

Research on Key Technologies for Anchor Methods in Pylon and π-Shaped Section Main Girder with Large Cantilevers of Huaizhou Tuojiang Bridge

Qiang Wang *, Yiyun Zhou, Kaisheng Feng, Shiwei Xiao and Zhiren Xiao

China Huaxi Engineering Design & Construction Co., Ltd., Chengdu 610031, Sichuan Province, China.
* Correspondence: 229929115@qq.com

Abstract: Taking the prestressed concrete cable-stayed bridge of the Huaizhou Tuojiang Bridge as the background, the numerical calculation method was used to analyze the effects of circular prestressing and steel anchor boxes on the load bearing of the concrete pylon wall. The results show that, for medium- and small-span cable-stayed bridges, setting up either a circumferential prestress or a steel anchor box system alone cannot effectively solve the problem of tensile cracking in the concrete pylon wall. However, the combined effect of both systems is better. Additionally, a numerical analysis method is used to calculate the shear lag effect of the π-shaped cross-section main girder with a large cantilever under the completed bridge state, studying the distribution pattern of normal stress in this type of section and providing a reference for the design of similar structures.

Keywords: cable-stayed bridge; pylon anchorage zone; circumferential prestress; steel anchor box; π-shaped section main girder; shear lag effect

Citation: Wang, Q.; Zhou, Y.; Feng, K.; Xiao, S.; Xiao, Z. Research on Key Technologies for Anchor Methods in Pylon and π-Shaped Section Main Girder with Large Cantilevers of Huaizhou Tuojiang Bridge. *Prestress Technology* **2024**, *4*, 54-68. https://doi.org/10.59238/j.pt.2024.04.004

Received: 22/10/2024
Accepted: 19/11/2024
Published: 30/12/2024

1 Introduction

The anchoring method of the pylon and the cross-sectional form of the main girder are two key aspects in the design of cable-stayed bridges. Selecting a reasonable design scheme is crucial for the overall design of cable-stayed bridges. The anchoring methods of cable-stayed bridge pylons can be classified into three main categories: circumferential prestress, steel anchor beams, and steel anchor boxes.

Circumferential prestress involves setting circumferential prestressing tendons in the pylon anchorage area to balance the internal forces generated by the cable tension, preventing cracks in the concrete due to horizontal component forces. This technology has been widely applied in China, with many successful experiences gained from full-scale model tests and structural analyses of numerous bridges. In particular, the emergence of vacuum grouting technology has largely resolved issues related to the grouting of circumferential prestressing tendons, leading to successful applications in several cable-stayed bridges, such as the Nanjing Yangtze River Second Bridge, Anqing Yangtze River Highway Bridge, and Junshan Yangtze River Highway Bridge.

The force transmission mechanism of the steel anchor beam is as follows: the steel anchor beam is supported on the corbels within the pylon walls, allowing slight movement and rotation in the horizontal plane. Horizontal limit devices are set at both ends of the steel anchor beam. The horizontal component forces of the cables are mainly borne by the cross-beam components of the steel anchor beam, whereas the unbalanced horizontal component forces between the two sides of the cables are transmitted to the pylon walls through friction or stop blocks between the steel anchor beam and the corbels, thereby significantly reducing the horizontal forces on the pylon walls.

The steel anchor box anchorage system, developed from a steel pylon and steel

https://doi.org/10.59238/j.pt.2024.04.004

anchor beam, although complex and less economical, provides a reliable anchorage and effectively solves the cracking problem of pylon concrete. Bridges such as the Hangzhou Bay Bridge, Nanjing Yangtze River Third Bridge, and Sutong Yangtze River Highway Bridge in China have adopted this type of anchorage [1]. Depending on the layout, steel anchor boxes can be categorized into an embedded scheme and a built-in scheme. In the embedded steel anchor box scheme, the arrangement of circumferential prestress tendons can effectively address the tensile issue of the pylon wall and enhance the overall integrity of the structure, improving the load-bearing condition of the shear studs. In the built-in steel anchor box, there are fewer cases where prestress is arranged. For example, the Xiangshan Harbor Bridge and the North Channel Bridge of the Hangzhou Bay Transoceanic Bridge have circumferential prestress tendons, whereas the Dongyang Yangtze River Bridge only sets transverse prestressing tendons at the end walls.

The main girders of cable-stayed bridges, depending on the material, can be classified into steel girders, concrete girders, composite girders, and hybrid girders. For medium- and small-span cable-stayed bridges, concrete main girders are commonly used. According to the section form, concrete main girders can be divided into separate double-box sections, single-box multicell sections, and π-shaped sections. Among these, the π-shaped section main girder, owing to its light self-weight and ease of construction, is often used in cable-stayed bridges, but it also has a significant shear lag effect.

In this study, the Huaizhou Tuojiang Bridge will be used to carry out detailed research on the above two issues.

2 Project Overview

Huaizhou Tuojiang Bridge is located in the urban area of Huaizhou town, Jintang County. The bridge span arrangement is as follows: (4×30) m + (4×30) m + (3×30) m + (155+120) m + (5×30) m + (4×30) m + (4×30) m + (4×30) m, for a total length of 1,119.0 m (including the length of the abutments at both ends). Among these, the 4th span main bridge crosses the Tuojiang River, utilizing a single-tower spatial double-cable plane prestressed concrete cable-stayed bridge design with spans of (155+120) m. The standard width of the main bridge is 33.0 m, the tower and pier are consolidated with a girder, and auxiliary piers are set up at the side spans. The completed Huaizhou Tuojiang Bridge is shown in Figure 1.

Figure 1 Huaizhou Tuojiang Bridge after being closed

The main girder of the main bridge has a π-shaped cross section, with a standard width of 33.0 m. A 7.5 m cantilever is set on the outer side of the main girder's side ribs, supported by transverse diaphragms. The center girder height is 2.7 m, and the side rib width is 2.0 m. The spacing of the stay cables on the girder is 6.5 m, and the spacing of the transverse diaphragms is 3.25 m, with a thickness of 0.3 m. The deck slab thickness is 0.28 m. The bridge type layout and cross-sectional arrangement of the main bridge are shown in Figures 2 and 3.

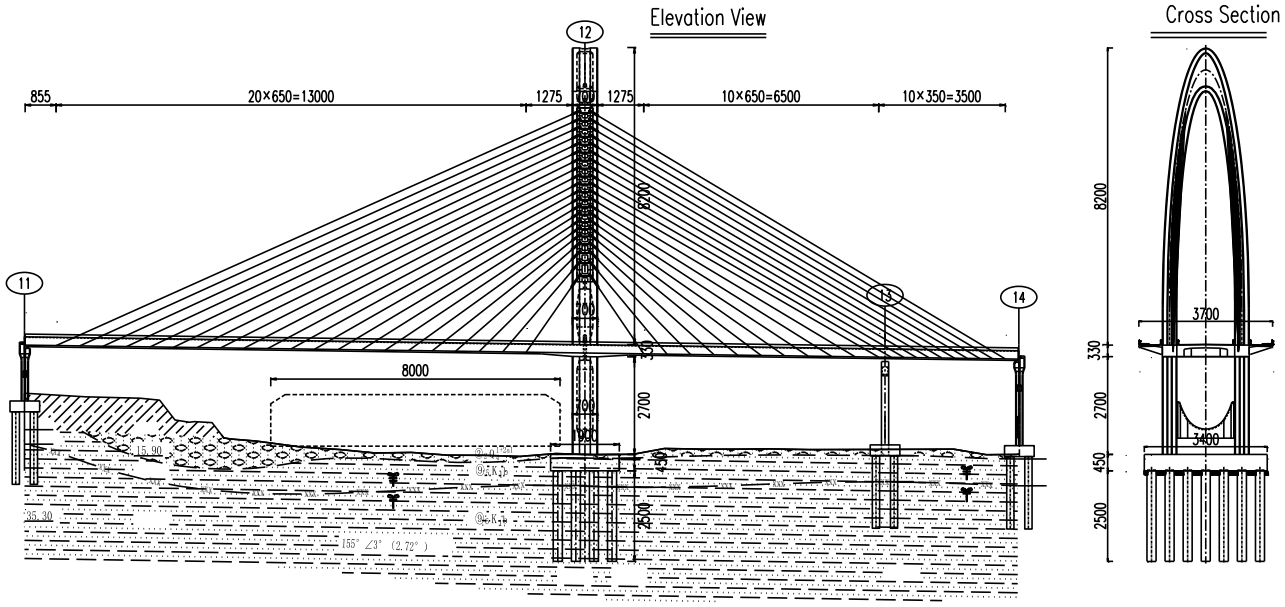

Figure 2 Schematic diagram of the bridge-type arrangement for the main bridge (Unit: cm)

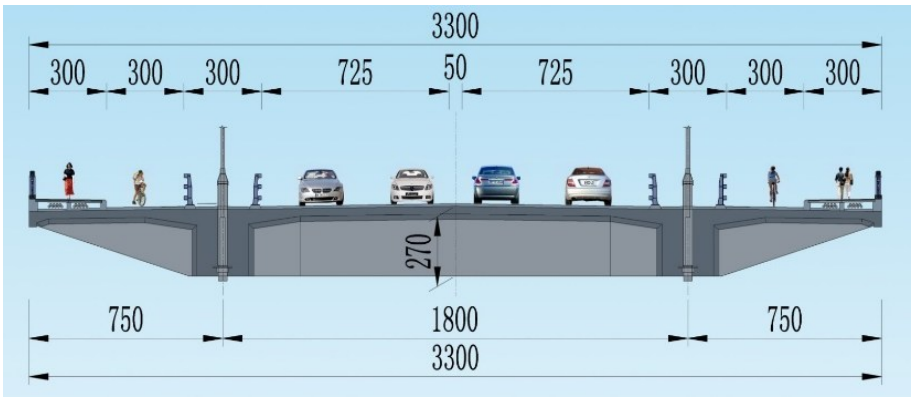

Figure 3 Schematic diagram of the cross-sectional layout of the standard section of the main bridge (Unit: cm)

The pylon adopts a reinforced concrete structure, with the upper pylon using a single-box single-cell rectangular hollow section. The wall thickness in the longitudinal direction of the bridge is 1.1 m, whereas it is 0.8 m in the transverse direction. The tower wall thickness within a certain range at the junction of the pylon beam consolidation section gradually increases. The vertical spacing of the stay cable anchor boxes at the tower end ranges from 2.0 m to 3.5 m. Steel anchor boxes and circumferential prestresses are arranged within the cable anchorage zone, as detailed in Figures 4 and 5.

 https://doi.org/10.59238/j.pt.2024.04.004

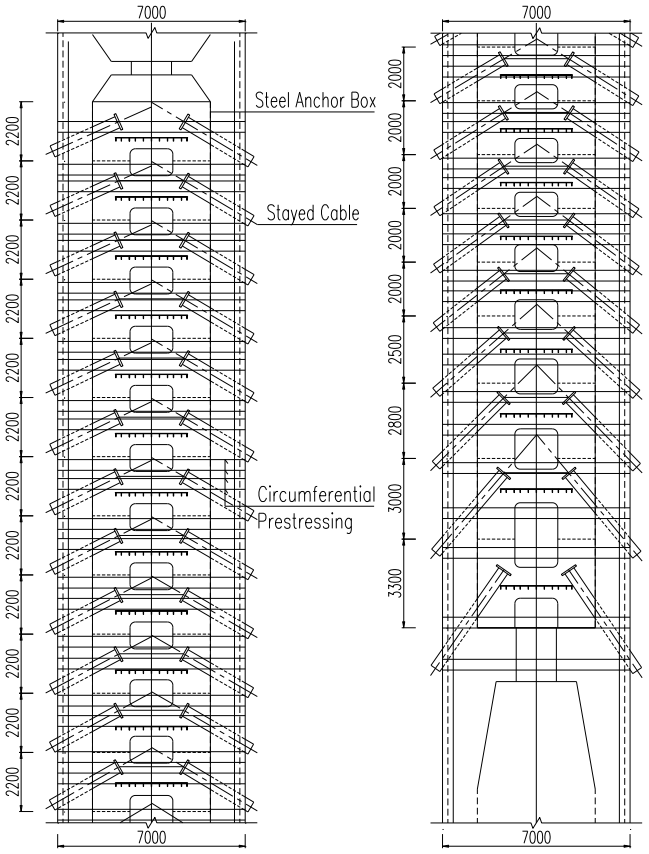

Figure 4 Elevation diagram of the steel anchor boxes and circumferential prestressing of the Huaizhou Tuojiang Bridge (Unit: mm)

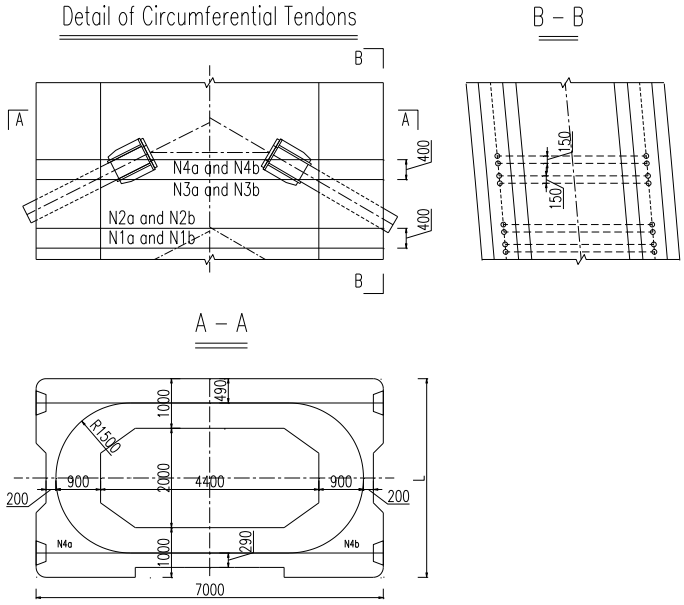

Figure 5 Arrangement detail of circumferential prestressing of the Huaizhou Tuojiang Bridge (Unit: mm)

3 Analysis of Force in the Pylon Anchorage Zone

3.1 Study on the Force Distribution Between a Steel Anchor Box and a Concrete Pylon Wall

The steel anchor box anchoring system mainly reduces the tensile force on the concrete pylon wall by allowing the steel anchor box to participate in load bearing. According to [2], for a rectangular pylon, reducing the aspect ratio of the pylon section, decreasing the wall thickness ratio, and increasing the area of the steel anchor

box's tension plate can lower the tensile force distributed to the concrete sidewall. The Huaizhou Tuojiang Bridge cable-stayed bridge is a medium- to small-span bridge [3] (in this paper, it generally refers to bridges with relatively small pylon dimensions where setting up a steel anchor box alone cannot effectively improve the stress condition of the concrete pylon). The pylon size and wall thickness are constrained by the scale and structural requirements of the bridge, making it difficult to meet the dimensional needs of a conventional steel anchor box for the concrete pylon wall. Therefore, further research is needed for the pylon of this project. A schematic diagram of the force mechanism analysis of the steel anchor box is shown in Figure 6.

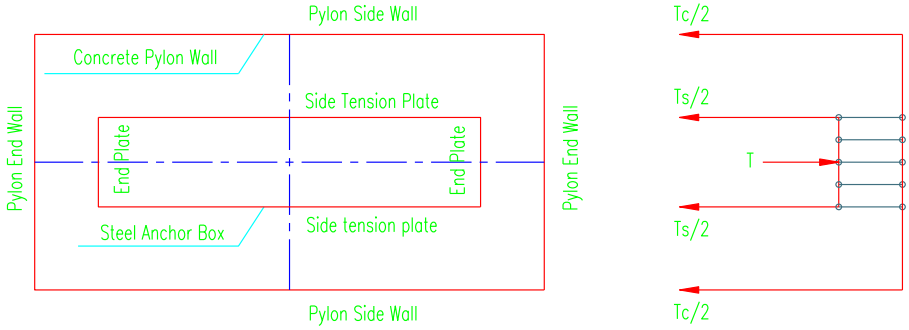

Figure 6 Diagram of the stress mechanism analysis of the steel anchor box

Figure 6 shows that the horizontal forces caused by the stay cables are borne by both the steel anchor box tension plates and the concrete sidewalls. By analyzing the forces on the steel anchor box and the concrete pylon wall, their deformations were calculated, as illustrated in Figure 7.

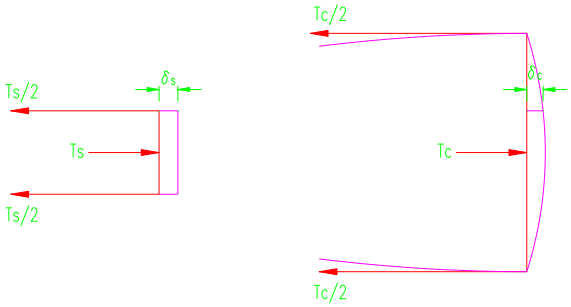

Figure 7 Diagram of deformation calculation of steel anchor box and concrete tower wall

Using the deformation calculation diagram in Figure 7, the deformation δ_s of the end plate of the steel anchor box and the deformation δ_c of the concrete end wall of the pylon were obtained. On the basis of the coordination relationship between the two deformations, an expression for the ratio of T_s (internal force in the side tension plate of the steel anchor box) and T_c (internal force in the longitudinal sidewall of the concrete pylon) was derived [4], as shown in Equation (1).

$$m = \frac{T_s}{T_c} = \frac{kb^3(4a+b)E_sA_s}{48(a+b)E_bI_b(a-d)} + \frac{a\mathrm{E}_sA_s}{E_cA_c(a-d)} \tag{1}$$

where E_b and I_b are the elastic modulus and moment of inertia of the end wall composite structure; E_s is the elastic modulus of the steel anchor box; A_s is the cross-sectional area of the steel anchor box side tension plate; E_c is the elastic modulus of the concrete; A_c is the cross-sectional area of the concrete sidewall; a and b are the longitudinal and transverse lengths of the pylon, respectively; d is the thickness of the concrete end wall; and k is the deformation conversion coefficient of the embedded steel anchor box (i.e., the ratio of the deformation at the coordination point between the concrete end wall and the steel anchor box end plate,

 https://doi.org/10.59238/j.pt.2024.04.004

$k = \delta_c/\delta_s$). The value of k can be determined through experimental methods, theoretical analysis, or simplified analytical models. In this work, a simplified analytical model method was used for calculation, which is detailed below.

First, a beam element simplified analysis model was established, with the longitudinal center of the steel anchor box and the concrete pylon wall as the axis of symmetry. Symmetrical boundary conditions were applied at the center of symmetry. Unit loads were applied to the actual force positions of the steel anchor box tension plate and the concrete pylon wall, and the deformations (δ_s and δ_c) of the steel anchor box and the concrete pylon end wall were calculated. Considering small deformations, the corresponding deformations under different tensile forces can be obtained.

Taking $T_s = 1, T_c = x$, the left side $m = T_s/T_c$ of Equation (1) is a function of x, as is the right side. By substituting $k = \delta_c/\delta_s$ into the right side of Equation (1) and manually adjusting the numerical values to make both sides equal, the deformation conversion coefficient k and the load distribution ratio m between the steel anchor box and the concrete can be obtained.

In the early stage of the scheme, the distribution ratio can be quickly calculated via the above method, which allows for a preliminary judgment of the rationality of the steel anchor box design. After calculation, the load distribution ratio for this bridge is 55:45 (m = 1.21; see Table 1), whereas the load common distribution ratio is 70:30. For this bridge, the concrete sidewall of the pylon bears too much tensile force, posing a risk of cracking; thus, the design needs to be optimized.

Table 1 Calculation table of distribution ratios between the steel anchor box and the concrete sidewall

Equation (1) left side			Equation (1) right side			
T_s	T_c	m	k	$\frac{kb^3(4a+b)E_sA_s}{48(a+b)E_bI_b(a-d)}$	$\frac{aE_sA_s}{E_cA_c(a-d)}$	m
1	0.825	1.21	1.55	0.87	0.34	1.21

To improve the tensile stress condition of the concrete sidewall of the pylon, the measure of adding circumferential prestress in the pylon was taken. Since the previous method cannot consider the influence of prestress, finite element analysis was used for the scheme with added circumferential prestress.

Similarly, a half model was established with the longitudinal center of the steel anchor box and the corresponding concrete pylon wall as the axis of symmetry, and symmetrical boundary conditions were applied at the center of symmetry. The calculation software used was Midas FEA NX (2024 R1), and the calculation model is shown in Figure 8.

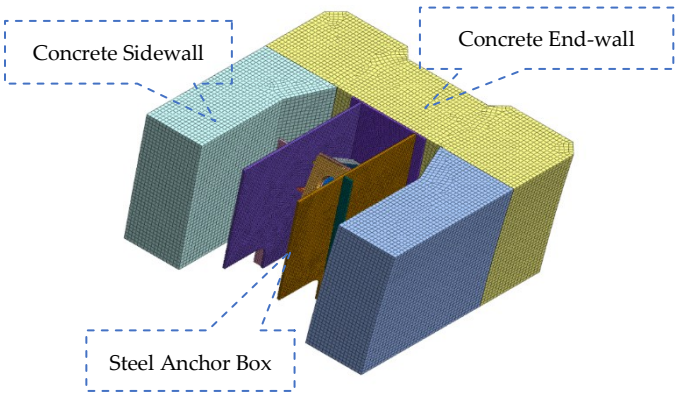

Figure 8 Schematic diagram of the calculation model

According to the detailed finite element model, the results without circumferential prestress were verified (Table 1). Under the force of the stay cables, the tensile

forces borne by the side tension plate of the steel anchor box and the concrete sidewall were 3568.6 kN and 2825.1 kN, respectively, with a distribution ratio of $m = 1.26$, which differs from the calculation result in Table 1 by 4.1%, showing good agreement.

3.2 *Analysis of the Influence of Circumferential Prestress on the Forces in the Concrete Pylon Wall and Steel Anchor Box*

After the circumferential prestress is applied, the prestress causes compressive deformation in the concrete sidewall, whereas the steel anchor box restrains this deformation and bears pressure. Owing to the addition of circumferential prestressing tendons, the concrete sidewall (including the prestressing tendons) bears more horizontal tensile force, whereas the tensile force borne by the steel anchor box side tension plate is reduced. After the circumferential prestress is applied, the load distribution ratio m between the steel anchor box and the concrete pylon wall changes to 24:76 ($m = 4.17$). The addition of circumferential prestress makes the load distribution ratio unsuitable for evaluating the effectiveness of the steel anchor box. At this point, stress analysis was conducted on the concrete sidewall, end wall, and side tension plate of the steel anchor box, and the results are shown in Figures 9 to 11.

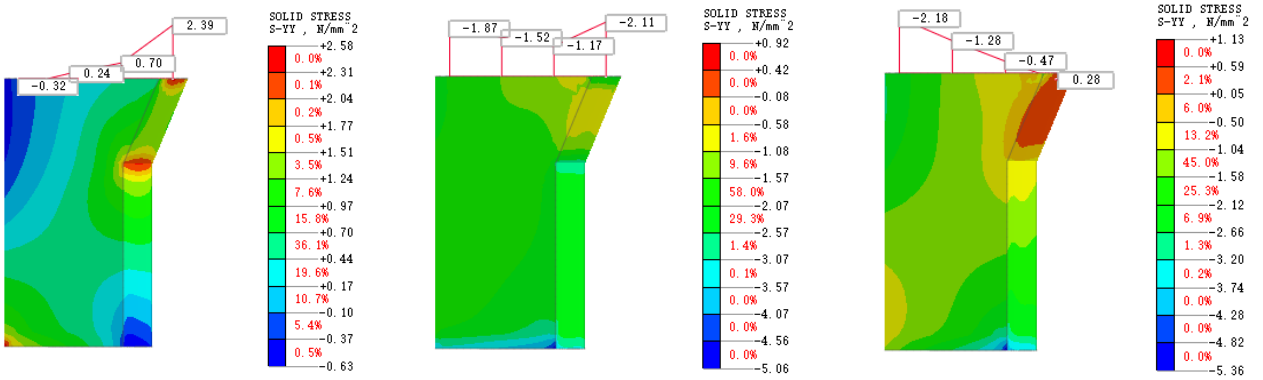

a) Stay cable force condition b) Circumferential prestress condition c) Combined action of stay cable force and circumferential prestress

Figure 9 Stress cloud diagram of the concrete sidewall root when a steel anchor box is set (Unit: MPa)

Figure 9 shows that without circumferential prestress, although the tensile force borne by the concrete sidewall is relatively small, a tensile stress of 2.39 MPa is generated at the inner side near the intersection of the concrete end wall and the concrete sidewall under the combined action of the bending moment and tensile force. The compressive stress caused by the bending moment on the outer side of the pylon wall is greater than the tensile stress caused by the tensile force, resulting in a net compressive stress of -0.32 MPa. The circumferential prestress produces a compressive stress of -1.06 to -2.11 MPa across the entire pylon wall section. Under the combined action of the stay cable force and circumferential prestress, the stress range at the root of the concrete pylon wall is -2.18 to 0.28 MPa.

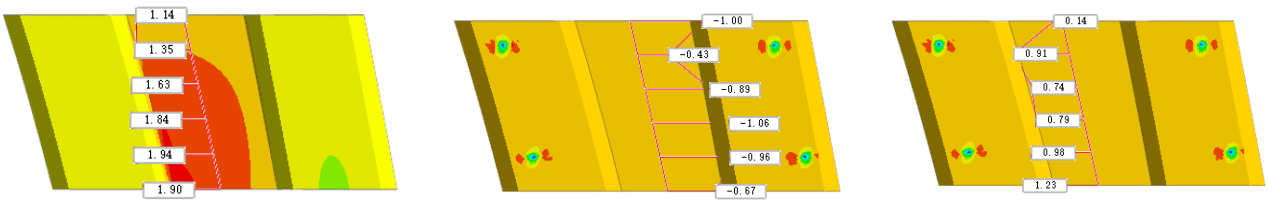

a) Stay cable force condition b) Circumferential prestress condition c) Combined action of stay cable force and circumferential prestress

Figure 10 Stress cloud diagram of the concrete end wall when a steel anchor box is set (Unit: MPa)

https://doi.org/10.59238/j.pt.2024.04.004

Figure 10 shows that under the action of the stay cables, the outer surface of the concrete end wall experiences significant tensile stress, reaching a maximum of 1.9 MPa. Under the action of circumferential prestress, the outer surface of the end wall produces a compressive stress of -0.43 to -1.06 MPa. Under the combined action of the stay cable force and circumferential prestress, the tensile stress on the outer surface of the end wall decreases, with a maximum of 1.23 MPa. Thus, applying circumferential prestress significantly reduces the tensile stress in the concrete pylon wall.

As mentioned earlier, after applying circumferential prestress, the steel anchor box constrains the deformation of the concrete sidewall, reducing the pressure effect of the prestress on the concrete pylon wall. Therefore, it is necessary to analyze the stress on the concrete pylon wall with only circumferential prestress tendons, and the results are shown in Figure 11.

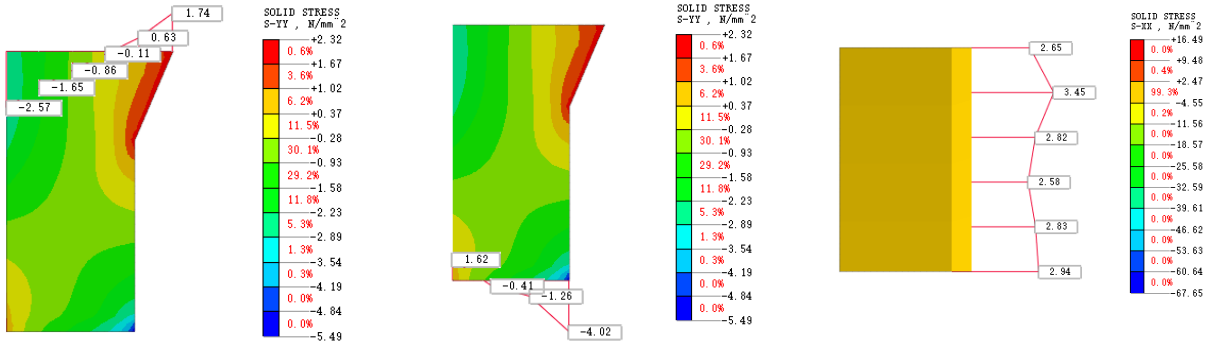

a) Stress cloud diagram of root section of the concrete sidewall

b) Stress cloud diagram of middle section of the concrete sidewall

c) Stress cloud diagram of middle section of the concrete end wall

Figure 11 Stress cloud diagram of the concrete pylon wall with only circumferential prestress tendons under the combined action of the stay cable force and circumferential prestress (Unit: MPa)

Figure 11 shows that with only circumferential prestress tendons, the stress distribution in the root and middle sections of the concrete sidewall is uneven under the combined action of the stay cable force and circumferential prestress. On the outer side of the root section, the stress is compressive, reaching -2.57 MPa, whereas on the inner side, it is tensile, reaching 1.74 MPa. In the middle section, the inner side shows compressive stress, reaching -4.02 MPa, whereas the outer side shows tensile stress, reaching 1.62 MPa. The concrete end wall exhibited overall tensile stress, with the maximum tensile stress reaching 3.45 MPa. Therefore, if only circumferential prestressing tendons are set, the stress conditions of the concrete pylon wall cannot be effectively improved. Large tensile stresses occur on the inner side of the root section, the outer side of the middle section, and the outer side of the end wall, indicating that the concrete is about to crack, affecting the durability and safety of the structure.

3.3 Summary

(1) For medium- and small-span cable-stayed bridges, owing to the limitations of the size and construction requirements of the concrete pylon wall, when the anchorage method at the pylon end is only the arrangement of a steel anchor box, the horizontal tensile force allocated to the concrete pylon sidewall is large, leading to high tensile stress, which makes it difficult to meet the tensile strength requirements.

(2) When only the circumferential prestress tendon scheme is adopted, it also cannot solve the problem of high tensile stress on the concrete pylon wall.

(3) The combination of steel anchor boxes and circumferential prestress technology improves the stress condition of the concrete pylon side and end walls, effectively solving the problem of excessive tensile stress in the anchorage zone of medium- and small-span cable-stayed bridges.

4 Study of the Shear Lag Effect of the π-Section Main Girder with a Large Cantilever

4.1 Theory of the Shear Lag Effect [5]

The design and calculation of cable-stayed bridges often use a frame model, where the internal forces of the structure are obtained through finite element analysis, and the components are checked via material mechanics methods. When verifying the strength of the main girder under normal service limit states, it is necessary to consider the effective distribution width of the upper and lower flange plates, which is essentially a shear lag effect issue.

For a π-shaped section of the main girder, owing to the nonuniformity of shear deformation in the flange plates, the longitudinal normal stress along the width of the flange plate exhibits a curved distribution. This phenomenon is referred to as the "shear lag effect." When the normal stress near the web of the flange plate is greater than that at the midpoint of the flange plate, it is called positive shear lag; conversely, it is called negative shear lag.

4.2 Model Establishment

A finite element model of the main span part of the main girder was established via Midas FEA. The connection between the pylon and the girder was modeled with fixed (constrained in six degrees of freedom) boundary conditions, whereas the actual boundary conditions were simulated at the beam end supports. The completed bridge cable forces were applied in the direction of the cables at the cable–beam connections. The work reported in this paper mainly studies the shear lag effect of the main girder under the action of dead load and cable forces during the final state of the bridge, as shown in Figure 12 for the calculation model.

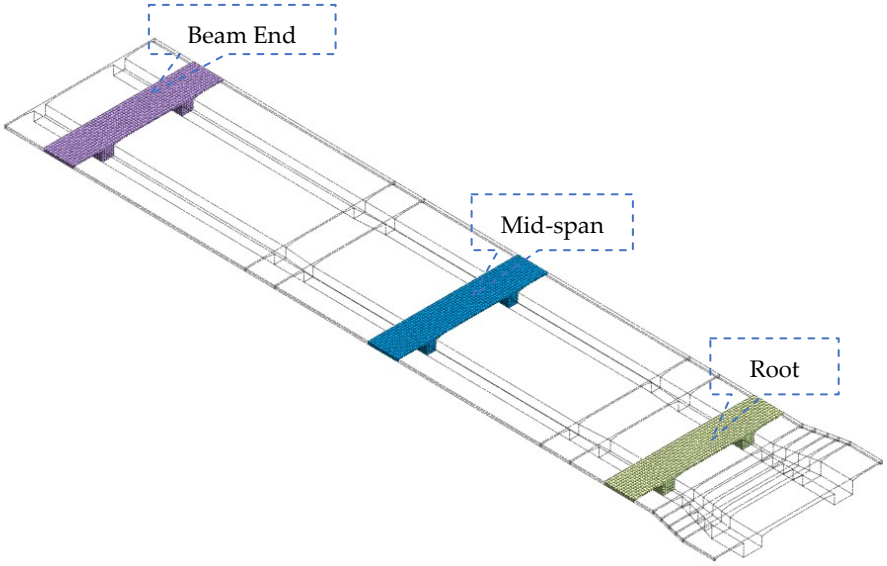

Figure 12 Schematic diagram of the calculation model for the main girder

To study the differences in the shear lag effect at different positions, three typical segments of the main girder were selected: the beam end, mid-span, and root, each segment being 6.5 m long, with the ends of each segment being the anchorage points of the stay cables, i.e., the points of action of the cable forces.

 https://doi.org/10.59238/j.pt.2024.04.004

4.3 Study on the Shear Lag Effect

The normal stresses at the center position of the top surface of the main girder for the beam end, mid-span, and root segments were extracted under the actions of dead load, completed bridge cable forces, and the combined action of dead load and completed bridge cable forces. The average values were calculated, and the extracted results were compared with the average values to analyze the influence of the shear lag effect on the stress distribution of the cross-section, as shown in Figures 13 to 15.

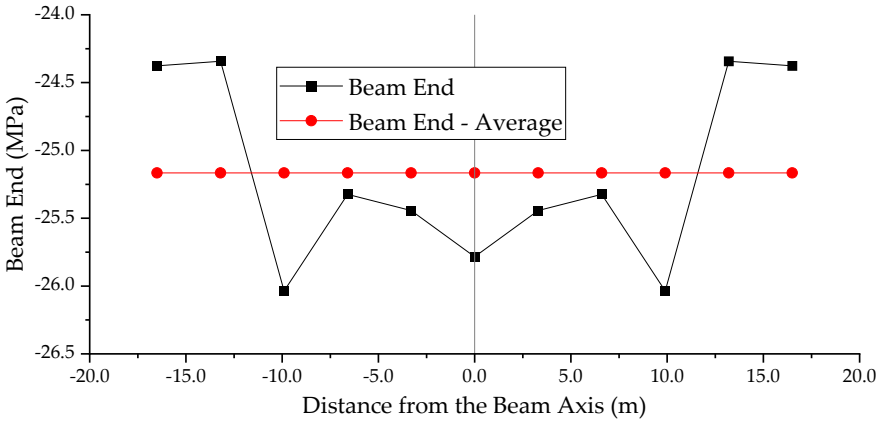

a) Stress distribution of the top surface of the beam end segment under dead load

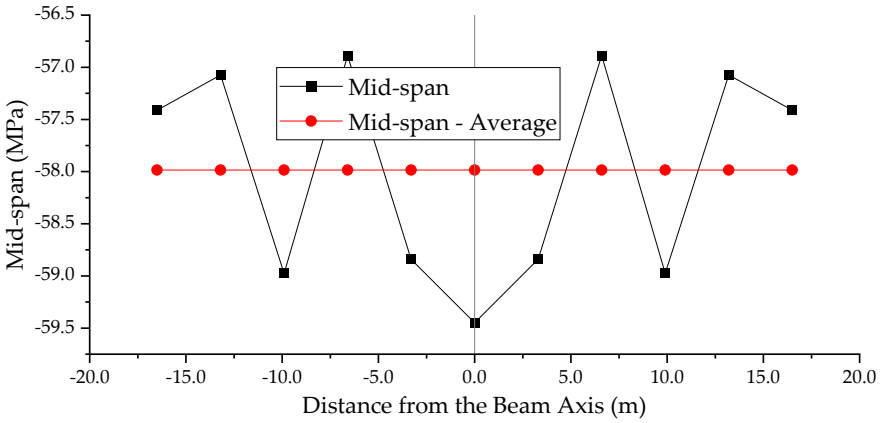

b) Stress distribution of the top surface of the mid-span segment under dead load

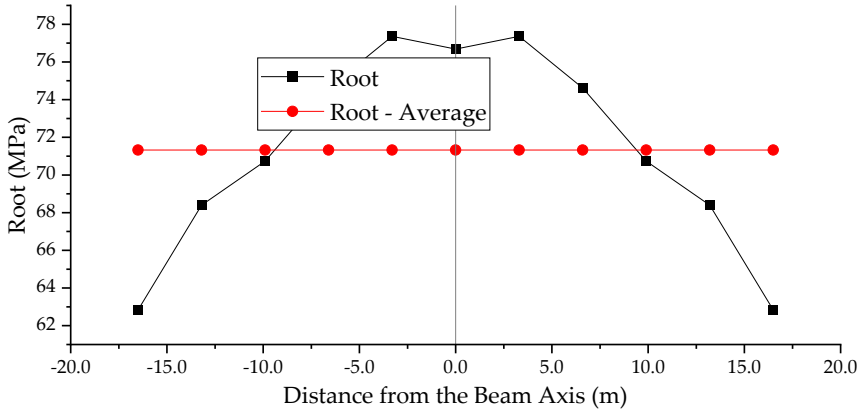

c) Stress distribution map of the top surface of the root segment under dead load

Figure 13 Normal stress distribution maps of the top surface of the main girder segments under dead load

Figure 13 shows that the normal stress distribution on the top surface of the main girder segments is uneven under the action of the dead load. In the beam end segment, the maximum normal stress occurs at the web, and the minimum occurs at the cantilever. The normal stress at the web and mid-span is greater than the average value and the normal stress at the cantilever being less than the average value. In the mid-span segment, there is a sudden change in the normal stress at the web, with the maximum normal stress at the mid-span and the minimum at the cantilever, where the normal stress is below the average value. In the root segment, the normal stress at the web is close to the average value, with the normal stress at the mid-span being higher than the average value, and the normal stress at the cantilever being lower than the average value. The normal stress distribution table for the top surface of the main girder segments under dead load is shown in Table 2.

Table 2 Normal stress distribution table for the top surface of the main girder segments under dead load (Unit: MPa) [6]

Distance from the beam axis (m)	Beam end	Beam end - average	Mid-span	Mid-span - average	Root	Root - average
-16.5	-24.4	-25.2	-57.4	-58.0	62.8	71.3
-13.2	-24.3	-25.2	-57.1	-58.0	68.4	71.3
-9.9	-26.0	-25.2	-59.0	-58.0	70.7	71.3
-6.6	-25.3	-25.2	-56.9	-58.0	74.6	71.3
-3.3	-25.4	-25.2	-58.8	-58.0	77.4	71.3
0.0	-25.8	-25.2	-59.4	-58.0	76.7	71.3
3.3	-25.4	-25.2	-58.8	-58.0	77.4	71.3
6.6	-25.3	-25.2	-56.9	-58.0	74.6	71.3
9.9	-26.0	-25.2	-59.0	-58.0	70.7	71.3
13.2	-24.3	-25.2	-57.1	-58.0	68.4	71.3
16.5	-24.4	-25.2	-57.4	-58.0	62.8	71.3

Table 2 shows that under the action of a dead load, the difference between the actual normal stress and the average value for the beam end segment is 0.9 MPa, that for the mid-span segment is 1.0 MPa, and that for the root segment is 8.5 MPa.

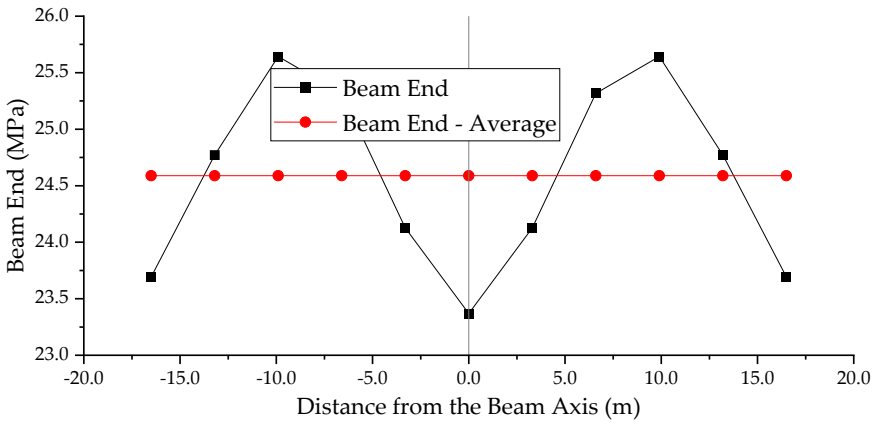

a) Stress distribution map of the top surface of the beam end segment

https://doi.org/10.59238/j.pt.2024.04.004

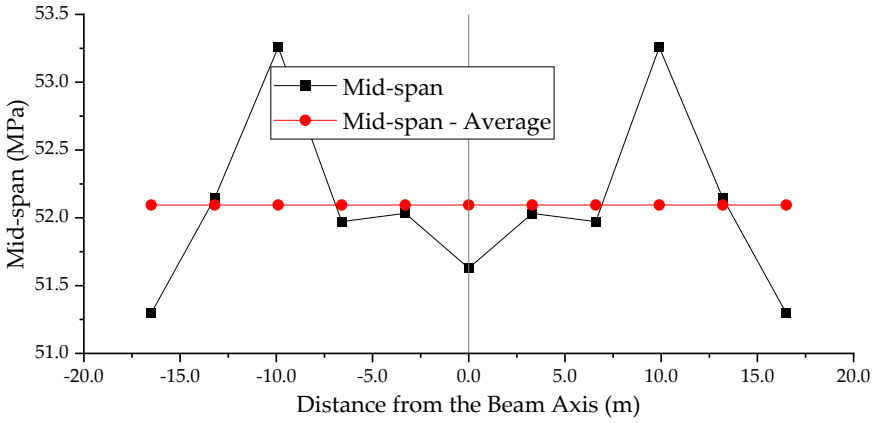

b) Stress distribution map of the top surface of the mid-span segment

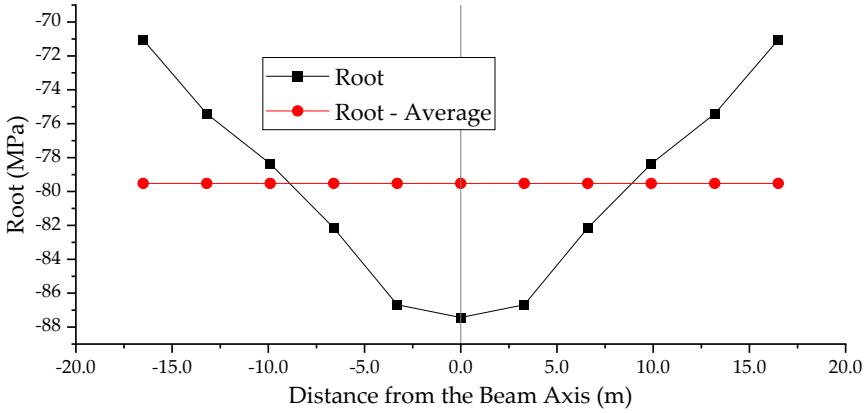

c) Stress distribution map of the top surface of the root segment

Figure 14 Normal stress distribution maps of the top surface of the main girder segments under completed bridge cable forces

Figure 14 shows that the normal stress distribution on the top surface of the main girder segments is also uneven under the action of the completed bridge cable forces. In the beam end segment, the maximum normal stress occurs at the web, with the normal stress at the web being greater than the average value and the normal stress at the cantilever and mid-span being less than the average value. In the mid-span segment, the stress distribution is like that of the beam end segment, with the maximum normal stress at the web, the minimum at the cantilever, and the mid-span stress being in between, with the normal stress at the web being greater than the average value, and the normal stress at the cantilever and mid-span being less than the average value. In the root segment, the normal stress at the web is close to the average value, with the normal stress at the mid-span being higher than the average value, and the normal stress at the cantilever being lower than the average value. The normal stress distribution table for the top surface of main girder segments under the action of cable forces is shown in Table 3.

Table 3 Normal stress distribution table for the top surface of the main girder segments under cable forces (Unit: MPa)

Distance from the beam axis (m)	Beam end	Beam end - average	Mid-span	Mid-span - average	Root	Root - average
−16.5	23.7	24.6	51.3	52.1	−71.0	−79.5
−13.2	24.8	24.6	52.1	52.1	−75.4	−79.5
−9.9	25.6	24.6	53.3	52.1	−78.4	−79.5
−6.6	25.3	24.6	52.0	52.1	−82.2	−79.5
−3.3	24.1	24.6	52.0	52.1	−86.7	−79.5

Distance from the beam axis (m)	Beam end	Beam end - average	Mid-span	Mid-span - average	Root	Root - average
0.0	23.4	24.6	51.6	52.1	−87.4	−79.5
3.3	24.1	24.6	52.0	52.1	−86.7	−79.5
6.6	25.3	24.6	52.0	52.1	−82.2	−79.5
9.9	25.6	24.6	53.3	52.1	−78.4	−79.5
13.2	24.8	24.6	52.1	52.1	−75.4	−79.5
16.5	23.7	24.6	51.3	52.1	−71.0	−79.5

Table 3 shows that under the action of completed bridge cable forces, the difference between the actual normal stress and the average value for the beam end segment is 1.2 MPa; for the mid-span segment, it is 1.2 MPa; and for the root segment, it is 8.5 MPa.

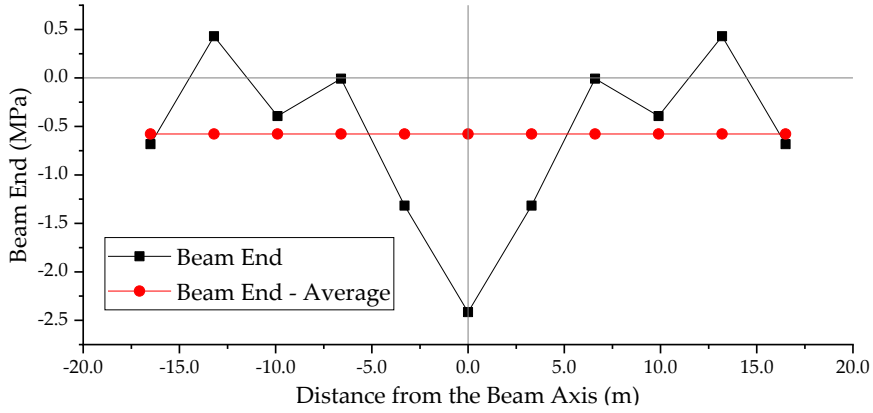

a) Stress distribution map of the top surface of the beam end segment

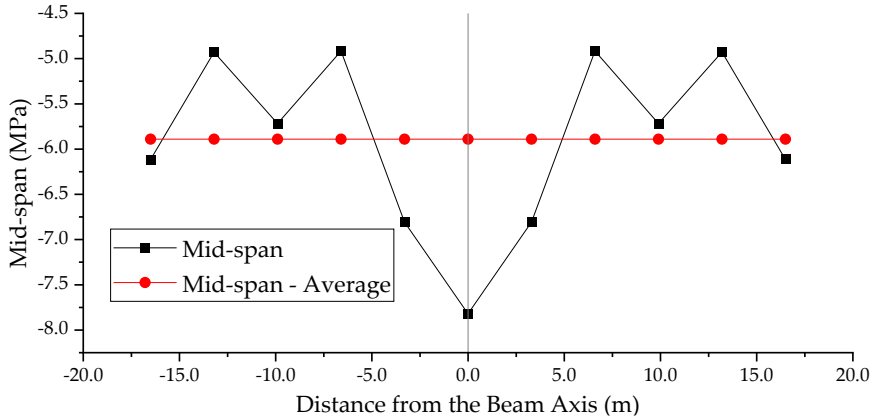

b) Stress distribution map of the top surface of the mid-span segment

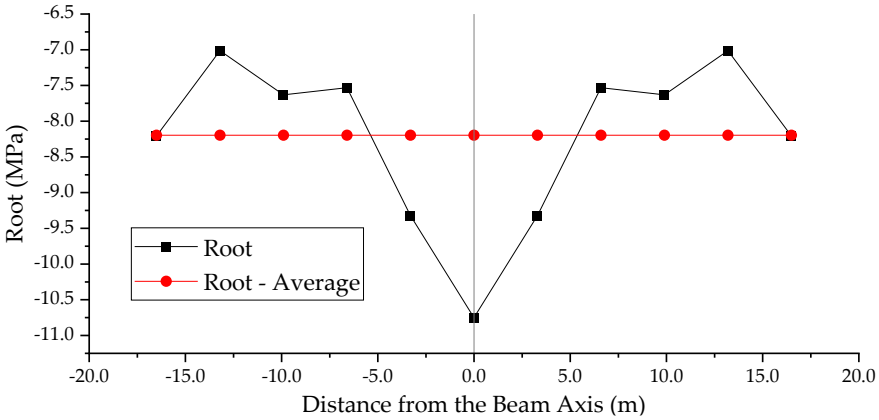

c) Stress distribution map of the top surface of the root segment

Figure 15 Normal stress distribution maps of the top surface of the main girder segments under the combined action of dead load and cable forces

https://doi.org/10.59238/j.pt.2024.04.004

Figure 15 shows that the normal stress distribution on the top surface of the main girder segments is uneven under the combined action of dead load and cable forces. In the beam end segment, the maximum normal stress occurs at the mid-span and it is greater than the average value, whereas the normal stress at the web and cantilever is smaller and less than the average value. The stress distributions in the mid-span and root segments are like to those in the beam end segment. The normal stress distribution table for the top surface of the main girder segments under the combined action of dead load and cable forces is shown in Table 4.

Table 4 Normal stress distribution table for the top surface of the main girder segments under the combined action of dead load and cable forces (Unit: MPa)

Distance from the beam axis (m)	Beam end	Beam end - average	Mid - span	Mid-span - average	Root	Root - average
−16.5	−0.7	−0.6	−6.1	−5.9	−8.2	−8.2
−13.2	0.4	−0.6	−4.9	−5.9	−7.0	−8.2
−9.9	−0.4	−0.6	−5.7	−5.9	−7.6	−8.2
−6.6	0.0	−0.6	−4.9	−5.9	−7.5	−8.2
−3.3	−1.3	−0.6	−6.8	−5.9	−9.3	−8.2
0.0	−2.4	−0.6	−7.8	−5.9	−10.8	−8.2
3.3	−1.3	−0.6	−6.8	−5.9	−9.3	−8.2
6.6	0.0	−0.6	−4.9	−5.9	−7.5	−8.2
9.9	−0.4	−0.6	−5.7	−5.9	−7.6	−8.2
13.2	0.4	−0.6	−4.9	−5.9	−7.0	−8.2
16.5	−0.7	−0.6	−6.1	−5.9	−8.2	−8.2

Table 4 shows that under the combined action of dead load and cable forces, the difference between the actual normal stress and the average value for the beam end segment is 1.8 MPa; for the mid-span segment, it is 1.9 MPa; and for the root segment, it is 2.6 MPa.

Having analyzed the completed bridge condition with the combined action of dead load and cable forces, the stress distribution of the cross-section caused by the shear lag effect does not significantly deviate from the average stress, with the maximum deviation being approximately 2.6 MPa. In the design, measures such as structural reinforcement or increasing the safety reserve of the structure should be taken for areas where the normal stress is greater than the average value.

5 Conclusions

With respect to the Huaizhou Tuojiang Bridge, this study examines the improved anchorage method at the pylon and the shear lag effect of the π-shaped main girder with a large cantilever, leading to the following conclusions. These research findings can serve as a reference for similar projects.

(1) For medium- and small-span cable-stayed bridges, owing to the limitations of the bridge scale and construction measures, setting up a steel anchor box alone makes it difficult to meet the force requirements and results in high tensile stress on the concrete. Setting up circumferential prestress alone would generate significant tensile stress on the inner side of the root section and the outer side of the middle section of the concrete pylon sidewall, as well as the outer side of the concrete pylon end wall. Neither approach alone can adequately address the high tensile stress on the concrete pylon wall, which affects the durability and safety of the structure.

(2) For medium- and small-span cable-stayed bridges, adopting an improved pylon anchorage method—combining circumferential prestress and steel anchor boxes—can effectively improve the stress conditions of the concrete pylon wall, making it primarily subjected to compression. For zones with minor tensile

stress, reinforcement can be increased to improve crack resistance, thus enhancing the durability and reliability of the concrete pylon wall.

(3) The π-shaped main girder with a large cantilever in this project will produce a certain degree of shear lag effect under the action of the bending moment perpendicular to the main girder, leading to an uneven normal stress distribution and some underestimation of stress. Measures such as increasing the safety reserve of the section strength and increasing the reinforcement can be taken to improve the stress conditions.

Conflict of Interest: All authors disclosed no relevant relationships.

Data Availability Statement: The data that support the findings of this study are available from the corresponding author, Wang, upon reasonable request.

References

1. Liu, S.; Wang, S. *Design of Cable-stayed Bridge*; China Communications Press: Beijing, 2006.
2. Zheng, Z.; Tong, Z. Mechanical and Parameter Analysis of Cable-to-Pylon Anchorage Zone with Built-in Steel Anchor Box. *Bridge Construction* **2009**, 61-66.
3. Ministry of Transport of the People's Republic of China JTG/T 3365-01—2020 Specifications for Design of Highway Cable-stayed Bridge. China Communications Press: Beijing, 2020.
4. Zheng, Z.; Tian, X.; Yu, J.; Kuang, X.; Wei, Q. Analysis of Mechanical Mechanism of Pylon Anchorage Zones with Built-in Steel-anchor-box. *China Journal of Highway and Transport* **2010**, *23*, 84-89, doi:10.3969/j.issn.1001-7372.2010.05.013.
5. Dai, W.; Xiao, W.; Yang, H.; Zhang, S. Shear Lag Effects of Cable-stayed Bridge with π-shape Cross-section Main Girder. *Journal of Transport Information and Safety* **2009**, *27*, 165-168, doi:10.3963/j.ISSN1674-4861.2009.04.039.
6. Zhang, Q.; Li, X.; Wu, J.; Liu, C. Study on the Tensioning Scheme for Construction Moni-toring of Asymmetric Single-Tower Cable-Stayed Bridges. *Prestress Technology* **2023**, *1*, 70-81, doi:10.59238/j.pt.2023.03.006.

AUTHOR BIOGRAPHIES

Qiang Wang
M.E., Senior Engineer. China Huaxi Engineering Design & Construction Co., Ltd.
Research Direction: Bridge Design and Research.

Email: 229929115@qq.com

Yiyun Zhou
D.Eng, Professor of Engineer. China Huaxi Engineering Design & Construction Co., Ltd.
Research Direction: Bridge Design and Research.

Email: 583509882@qq.com

Kaisheng Feng
B.E., Senior Engineer. China Huaxi Engineering Design & Construction Co., Ltd.
Research Direction: Bridge Design and Research.

Email: 463093501@qq.com

Shiwei Xiao
B.E., Senior Engineer. China Huaxi Engineering Design & Construction Co., Ltd.
Research Direction: Bridge Design and Research.

Email: swxiao2004@qq.com

Zhiren Xiao
B.E., Senior Engineer. China Huaxi Engineering Design & Construction Co., Ltd.
Research Direction: Bridge Design and Research.

Email: 446294577@qq.com

 https://doi.org/10.59238/j.pt.2024.04.004